

# A lattice dynamical treatment for the total potential energy of single-walled carbon nanotubes and its applications: relaxed equilibrium structure, elastic properties, and vibrational modes of ultra-narrow tubes

Jin-Wu Jiang,<sup>1</sup> Hui Tang,<sup>1</sup> Bing-Shen Wang,<sup>2</sup> and Zhao-Bin Su<sup>1,3</sup>

<sup>1</sup>*Institute of Theoretical Physics, Chinese Academy of Sciences, Beijing 100080, China*

<sup>2</sup>*State Key Laboratory of Semiconductor Superlattice and Microstructure*

*and Institute of Semiconductor, Chinese Academy of Sciences, Beijing 100083, China*

<sup>3</sup>*Center for Advanced Study, Tsinghua University, Beijing 100084, China*

In this paper, we proposed a lattice dynamic treatment for the total potential energy for single-walled carbon nanotubes (SWCNT's) which is, apart from a parameter for the non-linear effects, extracted from the vibrational energy of the planar graphene sheet. The energetics, elasticity and lattice dynamics are treated in terms of the same set of force constants independent of tube structures. Based upon the proposal, we investigated systematically the relaxed lattice configuration for narrow SWCNT's, the strain energy, the Young's modulus and Poisson ratio, and the lattice vibrational properties respected to the relaxed equilibrium tubule structure. Our calculated results for various physical quantities are nicely in consistency with existing experimental measurements. Particularly, we verified that the relaxation effect brings the bond length longer and the frequencies of various optical vibrational modes softer; Our calculation provides an evidence that the Young's modulus of armchair tube exceeds that of the planar graphene sheet, and the large diameter limits of the Young's modulus and Poisson ratio are in agreement with the experimental values of the graphite; The calculated radial breathing modes for the ultra narrow tubes with diameter range between 0.2 - 0.5 nm coincide the experimental results and the existing *ab initio* calculations with satisfaction; For narrow tubes of diameter 2 nm, the calculated frequencies of optical modes in tubule tangential plane as well as those of radial breathing modes are also in good agreement with the experimental measurement. In addition, our calculation shows that various physical quantities of relaxed SWCNT's can actually be expanded in terms of the chiral angle defined for the correspondent ideal SWCNT's.

PACS numbers: 81.07.De, 63.22.+m, 62.25.+g

## I. INTRODUCTION

After the discovery of the carbon nanotubes (CNT's) in 1991,<sup>1</sup> there have been several methods to prepare CNT's with ultra small diameters. Previously, CNT's were synthesized in a free space<sup>2,3</sup> and the quotient of narrow CNT's is quite low. Afterwards Z. K. Tang *et al.*<sup>4,5,6,7</sup> initiated to grow single-walled carbon nanotubes (SWCNT's) inside a channel of zeolite templates. The SWCNT's prepared in this way have the diameter as small as  $0.42 \pm 0.02$  nm. Actually there are three kinds of tubes with different chiralities in this diameter range: (5,0), (4,2), and (3,3). A fabrication process was further developed to prepare a type of samples with (5,0) and (3,3) only<sup>8</sup> with a very narrow diameter distribution. More recently, a stable CNT's with diameter 0.3 nm is found inside a multi-walled carbon nanotube.<sup>9</sup> As shown by the density functional studies<sup>9</sup> that this CNT might be interpreted as the armchair CNT (2,2) with a radial breathing mode (RBM) at  $787 \text{ cm}^{-1}$ . All these technological improvements stimulated progressively experimental and theoretical studies on the ultra narrow SWCNT's.<sup>10,11,12,13,14,15,16,17</sup>

Since the narrow CNT's possess biggish curvatures, the equilibrium geometries would deviate from the ideal geometry, i.e., deduced from a seamlessly rolling up planar graphitic lattice sheet referring to a chiral vector

$\vec{R} = n_1 \vec{a}_1 + n_2 \vec{a}_2$ .<sup>18</sup> Various methods have been developed to determine the equilibrium geometry of free SWCNT's.<sup>10,19,20,21,22</sup> Among others, in Ref. 10, the author calculated the total energy for narrow SWCNT's with a first-principles, all-electron, self-consistent local-density functional band-structure method. The calculated total energy can be parameterized in terms of five profitable parameters –i.e., generalized motif variables (GMV's)–with the line group symmetry intimately retained. The equilibrium geometry is obtained by an optimization procedure with respect to these GMV's. In Ref. 20, a molecular mechanical model for the effective total potential energy is proposed to calculate the equilibrium structure and the strain energy of achiral SWCNT's which is a quadratic form of lattice site displacements with respect to the planar graphite sheet. Apart from deviations of three bond lengths and three bond angles, a pyramidalization angle is introduced to describe the energy associated with the curvature. The calculated results are consistent with existing numerical results based on *ab initio* calculations.

Moreover, based upon the relaxed equilibrium geometry provided by *ab initio* method,<sup>10</sup> Milošević *et al.*<sup>11</sup> applied the line-group symmetry-based force constant method to calculate the vibrational modes of ultra-narrow SWCNT's, in which the fitted force constants of narrow SWCNT's have been adjusted with respect to the

provided cylindrical web geometry.

Besides, the elastic properties for carbon nanotubes have stimulated a large number of experimental and theoretical studies.<sup>23</sup> In particular, the Young's modulus is a significant physical quantity which reflects the striction of equilibrium structure in response to the impressed load. In Ref. 24, the axis Young's modulus of the SWCNT is measured as 1.2 Tpa by atomic force microscope technique. By observing their freestanding room-temperature vibrations in a transmission electron microscope,<sup>25</sup> the Young's modulus for 27 nanotubes in the diameter range 1.0 - 1.5 nm were measured and the average Young's modulus is 1.25-0.35/+0.45 Tpa.<sup>26</sup> An interesting fact was acknowledged that the Young's modulus of certain nanotubes is even higher than that of bulk graphite.

There have been a large number of theoretical calculations for the Young's modulus and the Poisson ratio. The *ab initio* method,<sup>21,27,28</sup> tight-binding approximation,<sup>29,30,31</sup> and force constant model<sup>32</sup> gave the results of Young's modulus with a range from 1 to 1.24 Tpa, and Poisson ratio in a range 0.16 - 0.27. It further shows that the calculated results vary slightly with different radii and chiralities. However, in Refs 33,34,35, 36, the calculated Young's modulus or the Poisson ratio are found to be chirality and tube radius-dependent. In Ref 33, the Poisson ratio of armchair tubes has the value larger than that of planar graphene sheet while for zigzag tubes smaller, and its planar sheet limit is 0.21. In Refs 34 and 35, the Poisson ratio decreases with increasing the tube diameter with the large diameter limit as 0.16. Anyhow, to our knowledge the resolution of the experimental measurements for the Young's modulus and Poisson ratio is still not enough satisfactory yet and the varies correspondent theoretical calculations are even more diverse.

As we have seen in above, *to figure out the total potential energy of SWCNT's as the functional of cylindrical lattice configuration is the key issue underlying the investigation of the equilibrium structure, strain energy, Young's modulus and lattice dynamics of ultra-narrow tubes.*

In this paper, we propose that the total potential energy for SWCNT's can be extracted from the vibrational energy of the planar graphene sheet with five force constants. In which the bi-linear forms of the lattice site displacements are accounted with the equilibrium lattice configuration of the planar graphite as the reference point, while one of the potential term for the twist motion needs to be improved by including a quartic term to account the non-linear effect. One of the advantages of our proposal is that the equilibrium structure, the elasticity, and the lattice dynamic properties for all kinds of SWCNT's are calculated in terms of the same set of six (5+1) force constants, which essentially reflects an unified microscopic mechanism founded on the five forms of motion of the graphite-type cylindrical lattice sheet. Based upon the proposal, we investigate systematically

the relaxed lattice configuration for narrow SWCNT's, the strain energy, the Young's modulus and Poisson ratio, and the lattice vibrational properties respected to the relaxed equilibrium tubule structure. The calculated results are nicely in consistency with the existing experimental measurements.

In particular, our calculation reveals a generic feature that the relaxation effect exhibits itself in stretching the bond lengths as well as softening the mode frequencies for all kinds of SWCNT's; It provides a kind of evidence that the Young's modulus of armchair tubes exceeds that of the planar graphene sheet, i.e., when the radius increases, the calculated values of the Young's modulus for armchair tubes approach that of the graphite from above and those of zigzag tubes from below. Meanwhile, the large diameter limits of the Young's modulus and Poisson ratio are in agreement with the experimental values of the graphite; The calculated RBM for the ultra narrow tubes with diameter range between 0.2 - 0.5 nm coincide the experimental results<sup>8</sup> and the existing *ab initio* calculations<sup>9</sup> with satisfaction. For narrow tubes of diameter 2 nm, the calculated frequencies of optical modes in tubule tangential plane as well as those of RBM are also in good agreement with the experimental measurement;<sup>37</sup> The honeycomb lattice symmetry-based chiral expansion for physical quantities of SWCNT's with ideal geometry<sup>38</sup> can be retained for those of relaxed SWCNT's by changing the chiral angle into its counterpart defined in tubes of ideal geometry; As expected, for tubes with diameter larger than approximately 0.8 nm where the relaxation effect dies away, the calculated frequencies and the sound velocities for various vibration modes are in accord with those of the tubes of ideal geometry.<sup>38</sup>

In Section II, the total potential energy for SWCNT's is presented, and the relaxed equilibrium geometry and correspondent strain energy are discussed. Section III is devoted to the lattice dynamics for ultra-narrow SWCNT's, while Section IV for the Young's modulus and Poisson ratio. Finally, the conclusion is in Section V.

## II. THE RELAXED EQUILIBRIUM STRUCTURE

### A. The geometry

We recall the geometrical description for the relaxed equilibrium structure of SWCNT's particularly for the ultra-narrow tubes following Ref. 10. As for the cylindrical coordinate description shown in Fig. 1, we first set the  $z$  axis along the tube axis, while the  $x$  axis is fixed passing through one of the  $A$  atoms. We further introduce a planar image of the cylindrical lattice sheet by unfolding the cylindrical tube into a planar lattice sheet, which is actually a tangential plane with the tangent line as a generatrix passing through the  $A$  atom, and set atom  $A$  as the origin of the plane with coordinates as  $(r_A, 0, 0)$ ,

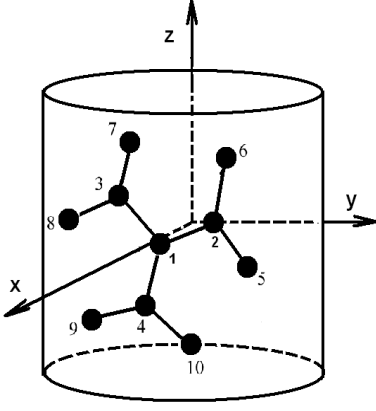


FIG. 1: Sketch of carbon atoms on a cylindric surface.

where  $r_A$  is the radius of atom  $A$ . The planar lattice sheet is constituted of parallelogram primitive cells with  $\vec{a}_1$  and  $\vec{a}_2$  as its basic vectors. The deviations of CNT's with relaxed geometry from that of ideal geometry can be illustrated most conveniently by the primitive cells on the image plane. For that of ideal geometry, the basic vectors are of equal magnitude with an intra-angle of  $\pi/3$  between themselves, while for that of the relaxed geometry, their magnitudes are no more equal and the angle can be deviated from  $\pi/3$ . Meanwhile, the location of the in-cell  $B$  atom relative to  $A$  atom could also be deviated from that of the ideal geometry.

Now we introduce the chiral vector  $\vec{R} = n_1\vec{a}_1 + n_2\vec{a}_2$  initiated from the atom  $A$  along the  $y$  axis in the image sheet, and  $R$  is the image circumference of cylindrical lattice sheet. We then introduce a screw vector  $\vec{H} = p_1\vec{a}_1 + p_2\vec{a}_2$  with integers  $p_1$  and  $p_2$  satisfying  $p_1n_2 - p_2n_1 = N$  and  $N$  is the largest common divisor of the integer pair  $(n_1, n_2)$ . Exactly following Refs 10 and 18,  $\vec{H}$  and  $\frac{\vec{R}}{N}$  constitute the basic ingredients of the generalized motif cell, upon which a generalized screw operation  $S(\alpha, h)$  and a generalized  $N$ -fold rotation operation  $C_N$  can be established. The former is a rotation  $\alpha$  around the tube axis with a simultaneous translation  $h$  along the tube axis, the latter a rotation of  $\frac{2\pi}{N}$  around the tube axis. A generalized motif cell  $(m, l)$  can be generated from the  $(0, 0)$  cell by successive operations of  $S(\alpha, h)$  and  $C_N$  for  $m$  and  $l$  times respectively. For the in-cell geometry of a generalized motif cell, originated from atom  $A$  the position of atom  $B$  can be fixed by a rotation  $\alpha'$  around the tube axis and two simultaneous translations  $h'$  and  $(r - r_A)$  along the tube axis and the tube radius respectively.

As a result, the coordinates on the cylindrical lattice sheet for each site  $(m, l, s)$  with  $s = A, B$  can be expressed as

$$\begin{aligned} \vec{r}(m, l, s) &= (r_s \cos \phi, r_s \sin \phi, z), \\ r_s &= r_A, \quad \phi = m\alpha + \frac{l}{N}2\pi, \quad z = mh \quad (\text{for } A), \end{aligned} \quad (1)$$

$$r_s = r, \quad \phi = m\alpha + \frac{l}{N}2\pi r + \alpha', \quad z = mh + h' \quad (\text{for } B).$$

While the corresponding coordinates in the image plane have the form as

$$\vec{r}^{\text{image}}(m, l, s) = (r_s, \phi r_s, z) \quad (2)$$

with the  $x$ -components of both  $A$  and  $B$  atoms as constants respectively.

Therefore, the six GMV's  $r, r_A, \alpha', h', \alpha$ , and  $h$  provide a complete description for the geometry of the lattice structure of SWCNT's, in which all the  $A$  and  $B$  atoms are allowed to sit on different cylindrical surfaces with radii  $r_A$  and  $r$  respectively.

## B. The total potential energy

In fact, in sense of quadratic approximation the vibration potential of the single layer graphite lattice sheet provides a proper description of various modalities of lattice motion. We, therefore, propose that the total potential energy of SWCNT's can be extracted from the vibration potential of graphene lattice sheet<sup>39</sup> as follows. Firstly, the total potential energy contributed by carbon atom 1, i.e., atom  $(0, 0, A)$ , is composed of the following five terms in which a local planar graphene sheet is taken as the reference point,

$$U_A = V_l + V_{sl} + V_{BB} + V_{rc} + V_{tw}, \quad (3)$$

where  $V_l$ ,  $V_{sl}$  are the potentials of the spring forces between the nearest-neighbor and the next-nearest-neighbor atom pair respectively as shown in Fig. 1,  $V_{BB}$  is the energy associated with bond angle variations,  $V_{rc}$  describes out-of-surface bond bending, i.e., a kind of strain force on atom  $i$  in out-of-surface direction by its three nearest neighbors in curling process, and  $V_{tw}$  is the twist potential energy.

$$V_l = \frac{k_l}{4} \sum_{i=2}^4 [(\Delta \vec{r}_i - \Delta \vec{r}_1) \cdot \vec{e}_{1i}^l]^2, \quad (4)$$

$$V_{sl} = \frac{k_{sl}}{4} \sum_{j=5}^{10} [(\Delta \vec{r}_j - \Delta \vec{r}_1) \cdot \vec{e}_{1j}^l]^2, \quad (5)$$

$$V_{BB} = \frac{k_{BB}}{2} \sum_{\eta=1}^3 (\cos \Theta_\eta - \cos \Theta_0)^2, \quad (6)$$

$$V_{rc} = \frac{k_{rc}}{2} \left[ \left( \sum_{i=2}^4 \Delta \vec{r}_i - 3\Delta \vec{r}_1 \right) \cdot \vec{e}_1^r \right]^2, \quad (7)$$

$$V_{tw} = \frac{k_{tw}}{4} \sum_{\langle i, j \rangle} f(x_{ij}^1), \quad (8)$$

$$x_{ij}^1 = [(\Delta \vec{r}_i - \Delta \vec{r}_j) - (\Delta \vec{r}_{i'} - \Delta \vec{r}_{j'})] \cdot \vec{e}_{1k}^r,$$

$$f(x) = \begin{cases} x^2 - K_{ah}x^4, & \text{if } |x| < \sqrt{\frac{1}{2K_{ah}}}, \\ \frac{1}{4K_{ah}}, & \text{if } |x| \geq \sqrt{\frac{1}{2K_{ah}}}. \end{cases}$$

In Eqs (4) to (8)  $i = 2, \dots, 4$  and  $j = 5, \dots, 10$  are the nearest and next-nearest neighbors of atom 1 respectively,  $\Theta_\eta$  with  $\eta = 1, 2, 3$  represent the three bond angles with atom 1 as the common apex while  $\Theta_0 = \frac{2\pi}{3}$  is the bond angle in the graphic plane,  $\langle i, j \rangle$  represents a pair of atoms nearest neighbored to atom 1 with  $k$  being the third of its nearest neighbors and the pair  $\langle i', j' \rangle$  is the image of  $\langle i, j \rangle$  referring to a  $C_2$  rotation around the axis in  $\vec{e}_{1k}^r$ . Moreover,

$$\Delta \vec{r}_i = \vec{r}_i - \vec{r}_i^0 \quad (9)$$

is the displacement of the carbon atom  $i$  from the planar graphene sheet  $\vec{r}_i^0$  to its counterpart in the tubal lattice sheet  $\vec{r}_i$ , in which  $i$  stands the site index  $(m, l, s)$  defined on the cylindrical lattice sheet. In addition,  $\vec{e}_{1i}^l = \frac{\vec{r}_i^0 - \vec{r}_1^0}{|\vec{r}_i^0 - \vec{r}_1^0|}$  is the unit vector pointed from atom 1 to atom  $i$  in the graphite sheet,  $\vec{e}_i^r$  and  $\vec{e}_{1k}^r$  are vertical unit vectors of the planar graphene sheet located at the site  $i$  and the middle point of sites 1 and  $k$  of the graphene sheet respectively. All the unit vectors are defined on the local reference graphene sheet and are introduced to keep the rigid rotational invariance symmetry. The above five potential terms in principle cover the main features of the modalities of lattice deformation suggested by Lianxi Shen *et al.*,<sup>20,34</sup> Chang *et al.*<sup>35</sup> in their mechanical model.

Correspondingly, that part of total potential energy in association with carbon atom  $B$   $(0, 0, B)$  has a similar expression as that of  $U_A$ , but with its geometrical parameters replaced by the counterpart of atom  $B$ .

Secondly, we express the lattice displacements in  $U_A$  and  $U_B$  in terms of the generalized motif variables. It spells that the locally constructed  $(0, 0)$  generalized motif cell with a pair of carbon atoms  $A$  and  $B$  can be continued to form a whole seamlessly closed cylindrical lattice sheet in which the generalized screw as well as rotation symmetries are inherited. As a result the total potential energy of SWCNT's has the form as a simple multiple of those associated with a pair of nearest neighboring atoms  $A$  and  $B$ , i.e.,  $U_A$  and  $U_B$  respectively,

$$U = \mathcal{N} * (U_A + U_B), \quad (10)$$

where  $\mathcal{N}$  is the number of generalized motif cells of SWCNT's in consideration. The redundant counting in the total potential energy contributed by different carbon atoms can be accounted by a proper resetting for the values of the relevant force constants. We further address that this sort of parameterization procedure can be carried out for all kinds of SWCNT's including both chiral and achiral tubes.

The values of force constants are  $k_l = 305 \text{ N m}^{-1}$ ,  $k_{sl} = 68.25 \text{ N m}^{-1}$ ,  $k_{BB} = 1.38 \times 10^{-11} \text{ erg}$ ,  $k_{rc} = 14.8 \text{ N m}^{-1}$ ,  $k_{tw} = 6.24 \text{ N m}^{-1}$ , and  $K_{ah} = 2.5$ . The frontal five force constants come from vibration energy of planar graphene sheet<sup>39</sup>. Since the twisting deformations increase substantially with decreasing the tube diameters, for example the twisting angle for the C-C bond can take the value as large as  $26^\circ$  for the narrow SWCNT  $(6, 3)$ ,

TABLE I: The calculating results of the five GMV's with  $r_A = \bar{r}$  and strain energy for narrow SWCNT's.

$(n_1, n_2)$	$r$ (Å)	$\alpha'$ (rad)	$h'$ (Å)	$\alpha$ (rad)	$h$ (Å)	$E_s$ (eV)
(2, 2)	1.743	1.1036	0.000	1.5708	1.255	1.5596
(3, 1)	1.817	1.0019	0.337	4.5923	0.580	1.7596
(4, 0)	1.977	0.7854	0.613	0.7854	2.033	1.3636
(3, 2)	2.013	0.8460	0.148	2.4777	0.491	0.7977
(4, 1)	2.129	0.7512	0.416	4.9317	0.455	0.8171
(3, 3)	2.281	0.7088	0.000	1.0472	1.238	0.4522
(5, 0)	2.283	0.6283	0.652	0.6283	2.069	0.6484
(4, 2)	2.333	0.6788	0.250	2.0127	0.803	0.4781
(5, 1)	2.458	0.6075	0.475	5.1657	0.376	0.4606
(4, 3)	2.593	0.6000	0.112	1.7827	0.351	0.3083
(6, 0)	2.617	0.5236	0.672	0.5236	2.089	0.3759
(5, 2)	2.673	0.5652	0.324	2.6560	0.339	0.3163

TABLE II: Contributions of five potential energy terms to the strain energy for tube  $(3, 3)$ .

$(3, 3)$	$V_l$	$V_{sl}$	$V_{BB}$	$V_{rc}$	$V_{tw}$
(eV)	0.02934	0.07191	0.02972	0.30179	0.01948

an additional force constant for the anharmonic improvement as  $K_{ah}$  in Eq. (8) has to be introduced. We notice here that the differences in lattice dynamics between such two types of systems are essentially due to their different spatial geometry, which are characterized by their own equilibrium lattice structure.

### C. The relaxed structure of SWCNT's

We introduce the total potential energy per atom as  $E$ ,

$$E = E(r, r_A, \alpha, h, \alpha', h') = (U_A + U_B)/2. \quad (11)$$

By minimizing  $E(r, r_A, \alpha, h, \alpha', h')$  with respect to the six GMV's, we obtain the optimized equilibrium geometry described by GMV's  $(\bar{r}, \bar{r}_A, \bar{\alpha}, \bar{h}, \bar{\alpha}', \bar{h}')$  as well as the strain energy  $E_s = E(\bar{r}, \bar{r}_A, \bar{\alpha}, \bar{h}, \bar{\alpha}', \bar{h}')$ . It is interesting to address that the optimized equilibrium lattice configurations for all tubes are shown to be of  $r_A = \bar{r}$ . This is because that the total energy  $U$  keeps unchanged when the tube is rotated upside down with atoms  $A$  and  $B$  mutually permuted, so that the optimized geometry must exhibit the  $C_2$  symmetry. The reflect symmetry  $\sigma_h$  with respect to the cross section is also kept for achiral tubes.

The calculated various lattice structure properties and the strain energies for narrow SWCNT's with diameter in  $[0.26, 0.5] \text{ nm}$  are listed in Table I, where the calculated GMV's are in good agreement with those by *ab initio* calculations.<sup>10</sup> Moreover, it is shown that the curvature energy associated with the fourth potential energy term

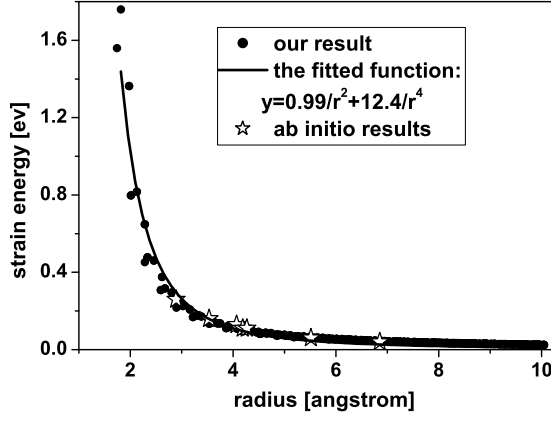


FIG. 2: The strain energy as the function of radius for all tubes in  $[1.3, 10.0]$  Å. It is compared with the *ab initio* calculations.<sup>20,21</sup>

in Eq. (7) dominates the total strain energy, while the corresponding contributions from the bond variation are usually much less than those from the bond angle variations (see Table II).

In Ref. 36, it is reported that the strain energy varies with tubule radius as  $\frac{1}{r^2}$  by applying the Tersoff-Brenner interatomic potentials. We here plot the strain energy versus radius in Fig. 2 which is comparable with the existing result<sup>21,36</sup> and can be well fitted by  $E_s = \frac{c_1}{r^2} + \frac{c_2}{r^4}$  in consistency with the result of Ref. 20. The coefficient of  $\frac{1}{r^4}$ —i.e.,  $c_2$ —is a bit large. That is because, in Ref. 20, there is no such twisting energy term as we have.

Our calculation shows that the radius and C-C bond lengths of CNT's of the optimized lattice configuration are always larger than those of the correspondent CNT's of the ideal geometry. We representatively display the three bond lengths in unit of the graphene bond length 0.142 nm for  $(2n, n)$  tubes with the relaxed geometry as well as ideal geometry in Fig. 3a. The relaxation, resulted from the optimization procedure, would disentangle the warping-induced tension and make the inter atomic bond length getting longer. To be precise, the bond lengths of the optimized lattice configuration decrease with increasing diameter and keep their values always larger than that of the graphene sheet. In contrary, for tubes of ideal geometry the bond lengths increase with increasing diameter and keep their values always smaller than that of the graphene sheet. As we can see in Fig. 3a, one of the bond lengths of the tube  $(4, 2)$  is 0.139 nm for ideal geometry while 0.157 nm for case of relaxed geometry which is about 11% more than that of the graphene sheet.

As shown in Fig. 3b, deviations of the bond angles from that of the graphene are really considerable for narrow tubes with diameter smaller than 0.8 nm. On the other hand, as can be seen in the same figure, this effect decreases quickly with increasing the tube diameter.

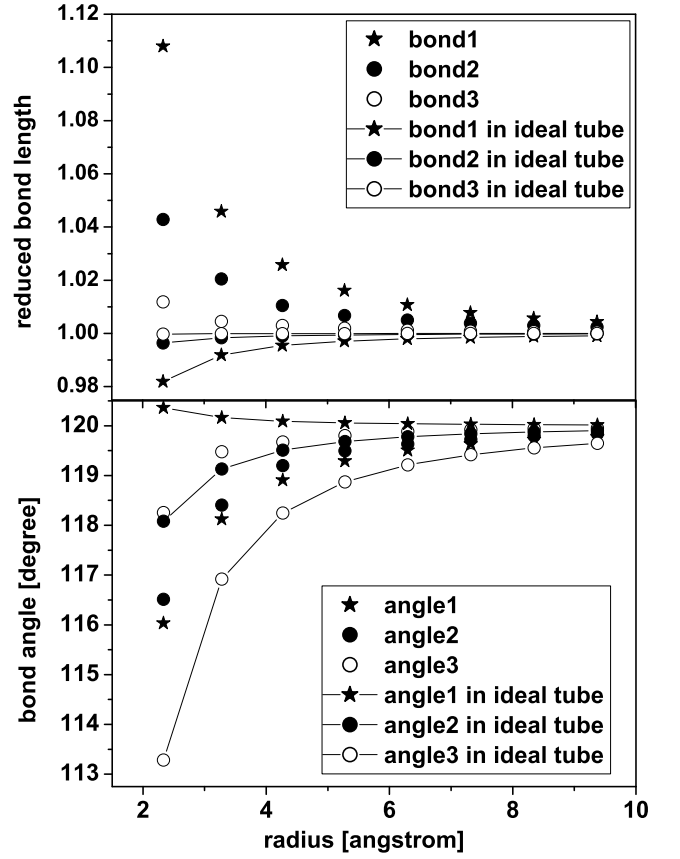


FIG. 3: C-C bond lengths reduced by that of graphite and bond angles for different chiral tubes  $(2n, n)$  with the relaxed geometry and ideal geometry.

### III. CALCULATION RESULTS AND DISCUSSION OF PHONON DISPERSION

In Sec. II, the relaxed equilibrium lattice configurations of SWCNT's are derived by an optimization procedure applied to the proposed total potential energy. The vibrational potential of SWCNT's is actually caused by the deviation of the lattice sites with respect to the relaxed equilibrium lattice configuration. It is obvious that the vibrational potential of SWCNT's would take the same form as the total potential energy, whereas the equilibrium position of the lattice site in the planar graphene sheet is therefore replaced by those in the relaxed cylindrical lattice sheet, meanwhile, the non-linear term is no more needed. The detailed modifications are as follows.

(1)  $\Delta \vec{r}_i = \vec{r}_i - \vec{r}_{i0}$  is renamed by convention as the vibrational displacement  $\vec{u}_i$  with  $\vec{r}_{i0}$  the local planar graphene sheet to be replaced by the relaxed equilibrium position of atom  $i$  in SWCNT's;

(2)  $\cos \Theta_0$  in Eq. (6) is no more the bond angle of graphene sheet as  $\frac{2}{3}\pi$  but the correspondent bond angle of the relaxed equilibrium configuration which depends on distinct adjacent atom pairs nearest neighbored to

the common apex atom  $i$ ;

(3)  $\vec{e}_{1i}^l$  and  $\vec{e}_{1j}^l$  are kept to be the unit vectors pointed from atom  $i$  and  $j$  to atom 1 respectively.  $\vec{e}_1^r$  is replaced

by  $\vec{e}_1^{rc} = -\frac{\sum_{i=2}^4 \vec{r}_{i0}}{|\sum_{i=2}^4 \vec{r}_{i0}|}$  and  $\vec{e}_{1k}^r$  becomes now the unit vector along the radial direction of the middle point of atoms 1 and  $k$ . We stress that all these unit vectors are defined on the cylindrical lattice sheet with optimized equilibrium geometry, which *taken a crucial role* to keep the rigid rotational invariance for the vibrational potential of relaxed SWCNT's;

(4) The coefficient  $K_{ah}$  is taken to be zero.

We emphase here that *the five force constants of the above proposed quadratic vibrational energy are the same as those in Sec IIB. They are applied to all kinds of SWCNT including those with small radii.* This is because that the rigid rotation symmetry of the SWCNTs is precisely kept. And the curvature effect for the vibrational modes has been properly taken care by the above introduced quadratic expression.

It is straightforward that such obtained vibrational potential can be again parameterized in terms of GMV's. Taking the advantage of GMV description for the cylindrical lattice configuration, the underlined generalized screw and rotation symmetries ensure that the lattice dynamic equation even for tubes with relaxed geometry can be decomposed into a six-dimensional eigenvalue problem and becomes treatable.

We calculate, for tubes with diameter from 0.28 nm to 2.5 nm, all the Raman- and Infrared-active modes,<sup>40</sup> and the velocities for the twisting modes (TW) and longitude acoustic modes (LA).

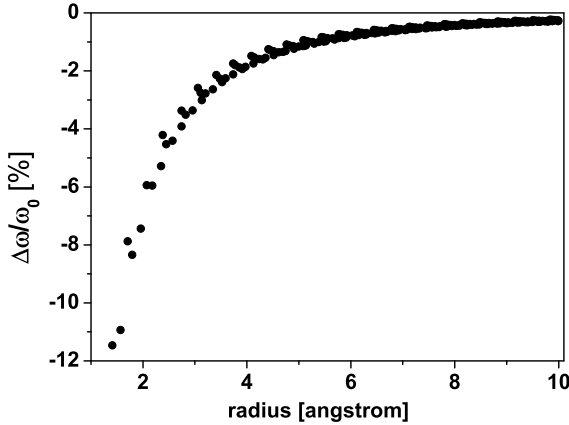


FIG. 4: The radius dependence of relative frequency change due to the relaxation effect for the optical mode along the  $z$  axis. The small waviness of the line shows the dependency of the frequencies on the chiral angle. For chiral and zigzag tubes this mode is the Raman-active mode.

The relaxation effect for the non-zero vibrational modes of the tubes with relaxed geometry exhibits itself as the frequency lowering (mode softening) in comparison with their counterpart of the tubes of ideal geometry.

TABLE III: The values of two optical modes in the tangential plane from our theory and compared with the experimental results.<sup>37</sup>

Optical mode	(11, 10)	(17, 9)	(27, 4)	(15, 14)
Our theory	1597.3	1600.5	1602.5	1602.1
	1600.7	1603.6	1605.5	1603.7
Experiment <sup>37</sup>	1566(7)	1572(13)	1577.5(10)	1573(7)
	1593.5(6)	1591(8)	1593(5)	1592(5)

TABLE IV: The values of RBM from our theory and compared with the experiments or other calculations.

RBM	(2, 2)	(5, 0)	(3, 3)	(4, 2)
Our theory	804.3	561.3	550.8	538.6
comparison	(787) <sup>a</sup>	(550) <sup>b</sup>	/	(510) <sup>b</sup>
RBM		(11, 10)	(16, 7)	(15, 6)
Our theory		160.0	142.5	155.2
comparison		(169.5(7)) <sup>c</sup>	(154(5)) <sup>c</sup>	(166(1)) <sup>c</sup>

<sup>a</sup>The *ab initio* calculations from Ref. 9; <sup>b</sup>The experiment results from Ref. 8; <sup>c</sup>The experiment results from Refs 37 and 41.

The effect of the relaxation on the optical mode along the  $z$  axis is shown in Fig. 4. The relaxation softens this mode considerably for narrow tubes. For example for the tubes with radius as narrow as 2 Å, this mode is softened as much as 8% in reference to that of the ideal geometry.

The calculated frequencies for the optical mode in the tubal tangential plane coincide excellently with the experimental measurements on tubes (11,10), (17,9), (27,4), (15,14),<sup>37</sup> see Table III. For the RBM, the calculated results from our model are in good agreement with

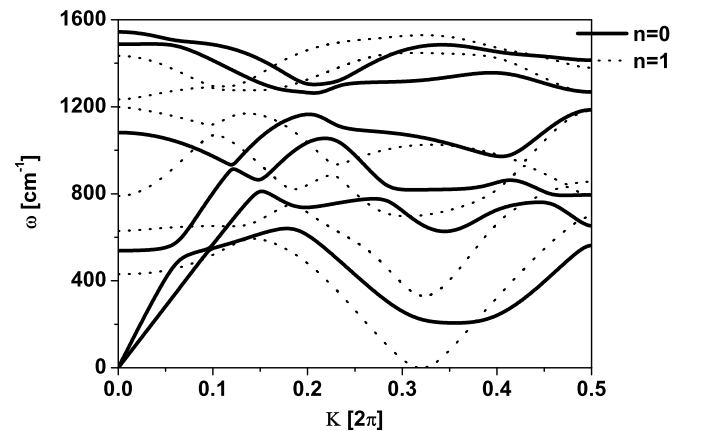


FIG. 5: Phonon dispersion curves for SWCNT (4,2) in the representation of helical and rotational quantum numbers. The flexure mode—i.e., the transversal acoustic mode—shows up at  $(\kappa, n) = (\alpha, 1)$ , where  $\alpha$  is in the unit of  $2\pi$ . It is double degenerate.

TABLE V: Polarization vectors  $\vec{u} \equiv (\vec{u}(A), \vec{u}(B))$  as functions of  $r$  ( $r \in [1.3, 10.0]$  Å) and  $\theta$ . Where  $\vec{u}(A)$  and  $\vec{u}(B)$  indicate the displacement vectors of atoms  $A$  and  $B$  in the  $(0, 0)$  unit cell respectively. For the three modes in this table,  $u_r(B) = u_r(A)$ ,  $u_\phi(B) = -u_\phi(A)$ ,  $u_z(B) = -u_z(A)$ .

$(\kappa, n) = (0, 0)$		Vector( $\theta$ )	$f_i(r)$
$R_1$ ( $\vec{e}_r$ AC)	$u_r(A)$	$f_0(r)$	$f_0(r) = 0.7072 - \frac{0.0026}{r^2}$
	$u_\phi(A)$	$f_1(r) \sin 3\theta$	$f_1(r) = -\frac{0.0212}{r} + \frac{0.1111}{r^2}$
	$u_z(A)$	$f_1(r) \cos 3\theta$	$f_1(r) = -\frac{0.0344}{r} + \frac{0.2167}{r^2}$
$R_2$ ( $\vec{e}_\phi$ OP)	$u_r(A)$	$f_1(r) \sin 3\theta$	$f_1(r) = \frac{0.0211}{r} - \frac{0.1064}{r^2}$
	$u_\phi(A)$	$f_0(r) + f_1(r) \cos 12\theta$	$f_0(r) = 0.6975 + \frac{0.0313}{r^2}$ , $f_1(r) = 0.0084 - \frac{0.0248}{r^2}$
	$u_z(A)$	$f_1(r) \sin 6\theta + f_2(r) \sin 12\theta$	$f_1(r) = 0.1642 - \frac{0.3742}{r^2}$ , $f_2(r) = -0.0283 + \frac{0.1512}{r^2}$
$R_3$ ( $\vec{e}_z$ OP)	$u_r(A)$	$f_1(r) \cos 3\theta$	$f_1(r) = \frac{0.0348}{r} - \frac{0.2189}{r^2}$
	$u_\phi(A)$	$f_1(r) \sin 6\theta + f_2(r) \sin 12\theta$	$f_1(r) = 0.1643 - \frac{0.3759}{r^2}$ , $f_2(r) = -0.0283 + \frac{0.1510}{r^2}$
	$u_z(A)$	$f_0(r) + f_1(r) \cos 12\theta$	$f_0(r) = 0.6975 + \frac{0.0299}{r^2}$ , $f_1(r) = 0.0084 - \frac{0.0236}{r^2}$

the correspondent results from the experiments on tubes (5, 0), (4, 2), (11, 10), (16, 7), (15, 6) listed in Table IV. Also for tube (2, 2) the calculate result is consistent with that of the *ab initio* calculation<sup>9</sup> (see Table IV). It can be seen moreover from Table IV that the smaller tube has the larger RBM frequency. This is consistent with some other calculation results.<sup>8,11</sup>

We take SWCNT (4, 2) as a typical example of the narrow tubes. Its dispersion is shown in Fig. 5 with the helical and rotational quantum numbers  $\kappa$  and  $n$  as  $n = 0, 1$  and  $\kappa \in [0, \pi]$ . In the neighborhood of  $(\kappa, n) = (0, 0)$ , there are two zero-frequency modes, TW and LA, with acoustic velocities as  $C_{TW} = 13.6$  km s<sup>-1</sup>, and  $C_{LA} = 20.7$  km s<sup>-1</sup> respectively. It is interesting to find that the  $C_{TW}$  is much smaller than that in the graphite plane. This effect is expected to be measured in experiments with technical developments. The frequencies of RBM,  $\vec{e}_r$  optical (OP) mode,  $\vec{e}_\phi$  OP mode and  $\vec{e}_z$  OP mode are calculated as 538.6, 1081.5, 1544.2 and 1487.7 cm<sup>-1</sup> respectively. At  $(\kappa, n) = \pm(\alpha, 1)$  with  $\alpha = 2.01$  radian, there are two transverse acoustic modes—i.e., the flexure modes—with the parabolic dispersions as  $\omega^2 = \beta^2(\kappa \mp \alpha)^4$  in the low-frequency limits. They are the consequence of the rotational invariance of our vibration potential.<sup>38,42</sup>

For tubes with diameter larger than approximately 0.8 nm where the curvature effect dies away, the calculated frequencies (Fig. 4), the sound velocities for various vibration modes, and even bond length (Fig. 3) etc. are in accord with those of the tubes of ideal geometry.<sup>38</sup> We notice that the slight difference in force constants between the present paper and Ref. 38 take no substantial effect on the lattice vibrational properties.

Although the lattice structure for the relaxed narrow SWCNT's deviates from that of the ideal geometry considerably, the chiral index  $(n_1, n_2)$  for the relaxed SWCNT's retains the symmetry information inherited from the hexagonal planar lattice sheet. As one might expect, our calculation verifies that various physical quantities can be expanded in terms of  $\cos 3n\theta$  and  $\sin 3n\theta$ ,  $n = 1, 2, \dots$ , with the same expansion forms as those

of the ideal geometry, in which  $\theta$  is the chiral angle defined for the correspondent tube with ideal geometry as  $\theta = \arctan \frac{\sqrt{3}n_2}{2n_1+n_2}$ . As an example, we show our fitted polarization vectors of RBM and two optical modes in tangential plane at  $(\kappa, n) = (0, 0)$  in Table V. The correspondent coefficients are shown almost the same as those in Table IV of Ref. 38.

#### IV. THE YOUNG'S MODULUS AND THE POISSON RATIO

The relaxed lattice configuration provides itself as the proper minimum of the total potential energy. In particular the equilibrium lattice configuration for the loaded SWCNT's can also be performed, which results that the calculation for various strain-induced physical quantities such as Young's modulus and Poisson ratio can be straightforwardly carried out. Among the GMV's,  $h$  and  $h'$  are the variables of the longitudinal degrees of freedom, while  $r$ ,  $\alpha$  and  $\alpha'$  are variables of peripheral degrees of freedom. However, the experimentally measured longitudinal stretching should correspond to the variable  $h$  while the variable  $h'$  essentially describes the microscopic in-cell displacement. The Young's modulus for the SWCNT's are introduced as:

$$Y = \left. \frac{\partial^2 E}{\partial \varepsilon_{11}^2} \right|_{\text{zero stress except the } (z, z) \text{ component}} \quad (12)$$

where  $\varepsilon_{11} = \frac{\Delta h}{h}$  being the longitudinal strain, and the derivatives are taken with all the other GMV's  $r, \alpha, \alpha'$  and  $h'$  being freely relaxed which corresponds to the boundary condition that all the components of stress tensor are zero except the  $(z, z)$  component. We stress that such a calculation of the Young's modulus for the cylindrical lattice sheet is consistent with the classical definition of Young's modulus in the continuum limit.<sup>43</sup>

TABLE VI: The large diameter limits of Young's modulus and Poisson ratio from our calculation and other existing results are compared with the experiment data.

	Experiment <sup>44</sup>	Our work	Theory <sup>a</sup>	Theory <sup>b</sup>	Theory <sup>c</sup>
$Y$ (eV)	56.43	56.3	60	69	53.3
$\mu$	0.17	0.166	0.19	0.25	0.277

<sup>a</sup>The *ab initio* method;<sup>21</sup> <sup>b</sup>The tight-binding approximation;<sup>29</sup> <sup>c</sup>The force constant model<sup>32</sup>

Accordingly the Poisson ratio

$$\mu = \left| \frac{\varepsilon_{22}}{\varepsilon_{11}} \right|_{\text{zero stress except the } (z, z) \text{ component}} \quad (13)$$

with  $\varepsilon_{22}$  being the peripheral strain induced under the same condition as explained above.

The calculated Young's modulus and Poisson ratio for various narrow SWCNT's can be well fitted as the functions of radius  $r$  and chiral angle  $\theta$ ,

$$Y = 56.3 - \frac{15.1 + 21.8 \cos 6\theta}{r^2}, \quad (14)$$

$$\mu = 0.166 + \frac{0.235 + 0.246 \cos 6\theta}{r^2}, \quad (15)$$

where  $Y$  is in the unit of eV,  $r$  is in the range of [1.3, 10] Å,  $\theta$  is the chiral angle defined for the correspondent SWCNT with ideal geometry as explained in the previous section, and the relative fitting error is kept less than  $1 \times 10^{-3}$ . As shown in Eqs (14) and (15), the Young's modulus and Poisson ratio in large diameter limit have the values of 56.3 eV and 0.166 respectively, which are in good agreement with the experimental results of graphite<sup>44</sup> (see Table VI). In the case of narrow tubes, they are significantly chirality-dependent. For example, the Young's modulus of three SWCNT's (3,3), (4,2), and (5,0) calculated as 57.74, 54.94, and 49.26 are considerably different from each other, although they have almost the same diameter.

Furthermore, we display the radius dependence of the Young's modulus in Fig. 6 for two species SWCNT's: armchair tubes  $(n, n)$ , and zigzag tubes  $(n, 0)$ . It shows clearly that the Young's modulus of armchair tubes decreases with increasing of tube diameter and always takes the values larger than that of planar graphite. While for zigzag tubes it exhibits a contrary behavior, i.e., increases with increasing diameter and keeps its value always below that of graphene sheet. It was reported in Ref. 26 that among 27 samples of carbon nanotubes, some of them are measured with the Young's modulus higher than that of bulk graphite. While, to our knowledge, most of the existing theoretical estimations<sup>45</sup> can only provide values of Young's modulus less than that of graphene sheet for any kind of SWCNT's. Our calculation provides an evidence that armchair tubes are stiffer while the zigzag softer due to the chirality-dependence.

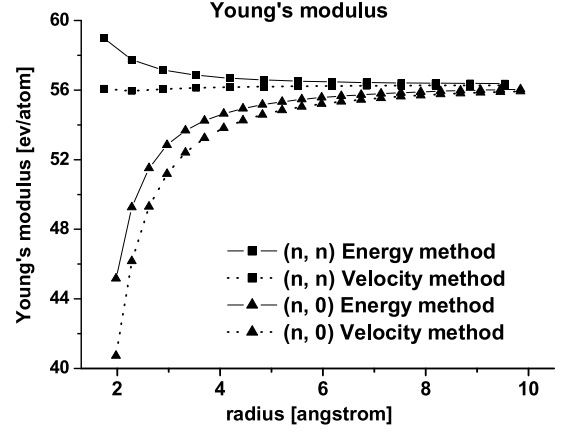


FIG. 6: The Young's modulus for armchair and Zigzag tubes. The lines are calculated by the second derivatives of energy per atom with respect to the uniform strain along the tubule axis direction. And the dashed lines are calculated by Eq (16) with velocity method.

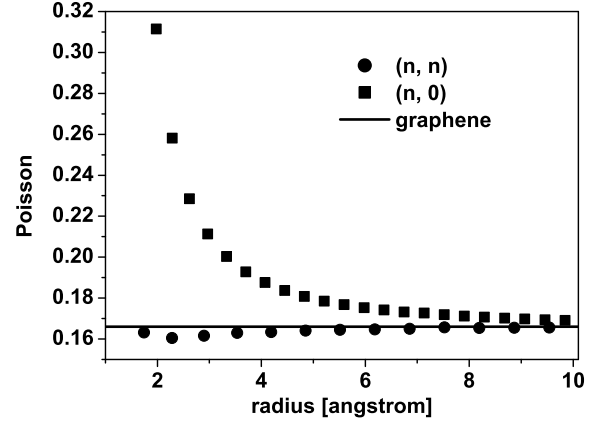


FIG. 7: The Poisson ratio for different armchair and zigzag tubes.

It is known that following the elasticity theory of the continuum medium, the Young's modulus as well as Poisson ratio can be derived from the relevant sound velocities,<sup>33,43</sup>

$$Y = \rho * V_L^2, \quad (16)$$

$$\mu = 0.5 * \left( \frac{V_L}{V_T} \right)^2 - 1, \quad (17)$$

where the two expressions are also referred to the boundary condition of only the  $(z, z)$  component of stress tensor being non-zero. Therefore, we may calculate the Young's modulus and Poisson ratio from the relevant sound velocities obtained in the last section shown in Fig. 6 for comparison. We emphasize that the Young's modulus (Poisson ratio) calculated from the strain energy following Eqs (12) and (13) and those calculated from the



sound velocities following Eqs (16) and (17) are essentially two distinct independent calculations. The former is in sense of a microscopic calculation following from the total potential energy Eqs (4)–(8), while the latter is a sort of macroscopic calculation with the sound velocities as its input although which is provided by the microscopic vibrational energy (introduced in section III). We can see from Fig. 6, for each of the two species of SWCNT ( $n, n$ ) and ( $n, 0$ ), the Young's module produced by the two kinds of calculations meet to each other closer and closer as the radius increases and have the correct  $r \rightarrow \infty$  limit as the experimental Young's modulus of graphite. Such a result arises from the intrinsic consistency between our total potential energy expression and that of the vibrational energy. The difference between the two kinds of calculations becomes apparent when tube radius decreases. We understand such a phenomenon as that the calculation following from the theory of elasticity is macroscopic in nature which would be failure for ultra narrow tubes.

We show the calculated Poisson ratios for armchair ( $n, n$ ) and zigzag ( $n, 0$ ) tubes in Fig. 7 as the function of radius. The values of the Poisson ratio are in an order as that those of zigzag are the largest and the armchair the smallest. This is consistent with the correspondent result of *ab initio* calculation.<sup>21</sup>

## V. CONCLUSIONS

In this paper, we proposed a lattice dynamic treatment for the total potential energy for SWCNT's which

is, apart from a parameter for the non-linear effects, extracted from the vibrational energy of the planar graphene sheet. Based upon the proposal, we investigated systematically the relaxed lattice configuration for narrow SWCNT's, the strain energy, the Young's modulus and Poisson ratio, as well as the lattice vibrational properties respected to the relaxed equilibrium tubule structure with the same set of force constants independent of tube structures. In particular, with the application of GMV's we not only successfully extend the locally introduced-total potential energy to the whole tube, but also make the lattice dynamics for SWCNT's with relaxed geometry becomes treatable. Comparing with the corresponding results obtained from the tubes with ideal geometry, we verified that the relaxation effect brings the bond length longer and the frequencies of various optical vibrational modes softer. Moreover, our approach not only deduces the proper large diameter limit values of Young's modulus and Poisson ratio, but also provides a strong evidence that SWCNT's with different chirality could be stiffer or softer than the planar graphene sheet. The calculated RBM and optical modes in tubule tangential plane are also in good agreement with the experimental measurements. In addition, we realized that the chiral symmetry-based general expansion formulae for different physical quantities survive for SWCNT's with relaxed geometry in the sense to replace the chiral angle by its counterpart defined in tubes of ideal geometry.

- 
- <sup>1</sup> S. Iijima, Nature (London) **354**, 56 (1991).
  - <sup>2</sup> R. Saito, G. Dresselhaus, and M. S. Dresselhaus, *Physical Properties of Carbon Nanotubes* (Imperial College Press, London, 1998).
  - <sup>3</sup> P. Nikolaev, M. J. Bronikowski, R. K. Bradley, F. Rohmund, D. T. Colbert, K. A. Smith, and R. E. Smalley, Chem. Phys. Lett. **313**, 91 (1999).
  - <sup>4</sup> Z. K. Tang, H. D. Sun, J. Wang, J. Chen, and G. Li, Appl. Phys. Lett. **73**, 2287 (1998).
  - <sup>5</sup> N. Wang, Z. K. Tang, G. D. Li, and J. S. Chen, Nature (London) **408**, 50 (2000).
  - <sup>6</sup> Z. M. Li, Z. K. Tang, H. J. Liu, N. Wang, C. T. Chan, R. Saito, S. Okada, G. D. Li, J. S. Chen, N. Nagasawa, and S. Tsuda, Phys. Rev. Lett. **87**, 127401 (2001).
  - <sup>7</sup> Y. F. Chan, H. Y. Peng, Z. K. Tang, and N. Wang, Chem. Phys. Lett. **369**, 541 (2003).
  - <sup>8</sup> Z. M. Li, Z. K. Tang, G. G. Siu, and I. Bozovic, Appl. Phys. Lett. **84**, 4101 (2004).
  - <sup>9</sup> X. Zhao, Y. Liu, S. Inoue, T. Suzuki, R. O. Jones, and Y. Ando, Phys. Rev. Lett. **92**, 125502 (2004).
  - <sup>10</sup> I. Cabria, J. W. Mintmire, and C. T. White, Phys. Rev. B **67**, 121406(R) (2003).
  - <sup>11</sup> I. Milošević, E. Dobardžić, and M. Damnjanović, Phys. Rev. B **72**, 085426 (2005).
  - <sup>12</sup> G. D. Li, Z. K. Tang, N. Wang, and J. S. Chen, Carbon **40**, 917 (2002).
  - <sup>13</sup> H. D. Sun, Z. K. Tang, J. Chen, and G. Li, Solid State Commun. **109**, 365 (1999).
  - <sup>14</sup> A. Jorio, A. G. Souza Filho, G. Dresselhaus, M. S. Dresselhaus, A. Righi, F. M. Matinaga, M. S. S. Dantas, M. A. Pimenta, J. Mendes Filho, Z. M. Li, Z. K. Tang, and R. Saito, Chem. Phys. Lett. **351**, 27 (2002).
  - <sup>15</sup> P. Launois, R. Moret, D. Le Bolloch, P. A. Albouy, Z. K. Tang, G. Li, and J. Chen, Solid State Commun. **116**, 99 (2000).
  - <sup>16</sup> Z. K. Tang, H. D. Sun, and J. Wang, Physica B **279**, 200 (2000).
  - <sup>17</sup> M. Hulman, H. Kuzmany, O. Dubay, G. Kresse, L. Li, and Z. K. Tang, J. Chem. Phys. **119**, 3384 (2003).
  - <sup>18</sup> C. T. White, D. H. Robertson, and J. W. Mintmire, Phys. Rev. B **47**, 5485 (1993).
  - <sup>19</sup> J. Kürti, G. Kresse, and H. Kuzmany, Phys. Rev. B **58**, R8869 (1998).
  - <sup>20</sup> Lianxi Shen and Jackie Li, Phys. Rev. B **71**, 165427 (2005).
  - <sup>21</sup> Daniel Sánchez-Portal, Emilio Artacho, José M. Soler, Angel Rubio, and Pablo Ordejón, Phys. Rev. B **59**, 12678 (1999).
  - <sup>22</sup> V. N. Popov, L. Henrard, and P. Lambin, Phys. Rev. B

- 72**, 035436 (2005).
- <sup>23</sup> E. W. Wong, P. E. Sheehan, and C. M. Lieber, *Science* **277**, 1971 (1997).
  - <sup>24</sup> T. W. Tombler, C. Zhou, J. Kong, H. Dai, L. Liu, C. S. Jayanthi, M. Tang, and S. Y. Wu, *Nature (London)* **405**, 769 (2000).
  - <sup>25</sup> M. M. J. Treacy, T. W. Ebbesen, and J. M. Gilson, *Nature (London)* **381**, 678 (1996).
  - <sup>26</sup> A. Krishnan, E. Dujardin, T. W. Ebbesen, P. N. Yianilos, and M. M. J. Treacy, *Phys. Rev. B* **58**, 14 013 (1998).
  - <sup>27</sup> G. Van Lier, C. Van Alsenoy, V. Van Doren, and P. Geerlings, *Chem. Phys. Lett.* **326**, 181 (2000).
  - <sup>28</sup> G. Zhou, W. Duan, and B. Gu, *Chem. Phys. Lett.* **333**, 344 (2001).
  - <sup>29</sup> E. Hernández, C. Goze, P. Bernier, and A. Rubio, *Phys. Rev. Lett.* **80**, 4502 (1998).
  - <sup>30</sup> J. M. Molina, S. S. Savinsky, and N. V. Khokhriakov, *J. Chem. Phys.* **104**, 4652 (1996).
  - <sup>31</sup> Zhou Xin, Zhou Jianjun, and Ou-Yang Zhong-can, *Phys. Rev. B* **62**, 13692 (2002).
  - <sup>32</sup> J. P. Lu, *Phys. Rev. Lett.* **79**, 1297 (1997).
  - <sup>33</sup> V. N. Popov, V. E. Van Doren, and M. Balkanski, *Phys. Rev. B* **61**, 3078 (2000).
  - <sup>34</sup> L. Shen and J. Li, *Phys. Rev. B* **69**, 045414 (2004).
  - <sup>35</sup> Tienchong Chang *et al.*, *Appl. Phys. Lett.* **87**, 251929 (2005).
  - <sup>36</sup> D. H. Robertson, D. W. Brenner, and J. W. Mintmire, *Phys. Rev. B* **45**, 12592(R) (1992).
  - <sup>37</sup> M. Paillet, T. Michel, J. C. Meyer, V. N. Popov, L. Henrard, S. Roth, and J. -L. Sauvajol, *Phys. Rev. Lett.* **96**, 257401 (2006).
  - <sup>38</sup> J. W. Jiang, H. Tang, B. S. Wang, and Z. B. Su, *Phys. Rev. B* **73**, 235434 (2006).
  - <sup>39</sup> T. Aizawa, R. Souda, S. Otani, Y. Ishizawa, and C. Oshima, *Phys. Rev. B* **42**, 11469 (1990); **43**, 12060(E) (1991). There are slight differences between our five force constants and those of Aizawa *et al.* which does not make sense for description of the lattice dynamics of planar graphene sheet.
  - <sup>40</sup> Ofir E. Alon, *Phys. Rev. B* **63**, 201403(R) (2001).
  - <sup>41</sup> Jannik C. Meyer, Matthieu Paillet, Thierry Michel, Alain Moreac, Anita Neumann, Georg S. Suesberg, Siegmur Roth, and Jean-Louis Sauvajol, *Phys. Rev. Lett.* **95**, 217401 (2005).
  - <sup>42</sup> G. D. Mahan and Gun Sang Jeon, *Phys. Rev. B* **70**, 075405 (2004).
  - <sup>43</sup> L. D. Landau, and E. M. Lifshitz, *Theory of Elasticity* (Pergamon, Oxford, 1995).
  - <sup>44</sup> O. L. Blakslee, D. G. Proctor, E. J. Seldin, G. B. Spence, and T. Weng, *J. Appl. Phys.* **41**, 3373 (1970).
  - <sup>45</sup> Nan Yao and Vincenzo Lordi, *J. Appl. Phys.* **84**, 1939 (1998); this work was referred by T. Xiao and K. Liao, *Phys. Rev. B* **66**, 153407 (2002).